COBEM 2021 26th International Congress of Mechanical Engineering
November 22-26, 2021, Virtual Congress, Brazil
ABCM Associação Brasileira de Engenharia e Ciências Mecânicas

COB-2021-1442
EVALUATION AND MODELING OF THE PART-LOAD PERFORMANCE OF A BIOMASS STEAM GENERATOR INTEGRATED WITH A CONCENTRATED SOLAR POWER PLANT

Álvaro A. Díaz Pérez
Federal University of Santa Catarina (UFSC), Florianópolis, Brazil
alvaro@labcet.ufsc.br
Eduardo Konrad Burin
Federal University of Paraná (UFPR), Palotina, Brazil
eduardo.burin@ufpr.br
Edson Bazzo
Federal University of Santa Catarina (UFSC), Florianópolis, Brazil, alvaro@labcet.ufsc.br
e.bazzo@ufsc.br

Abstract. *Hybrid systems involving the use of biomass and solar energy have been proposed as a promising alternative to reduce greenhouse gas emissions in the generation of heat and electricity. This integration provides a way to overcome the inherited shortcomings of solar energy, such as intermittent and instability. Nevertheless, it might be observed that some plant components will operate in the off-design condition once solar energy is added to the cycle, penalizing their performance at partial loads. In this regard, the objective of this work is to evaluate the performance of an existing biomass steam generator at partial loads, integrated with a Fresnel solar field on fuel-saving mode. The equipment consists of a biomass steam generator fueled with eucalyptus woodchips with a capacity to produce up to 50 t/h of superheated steam at 420 °C / 45 bar(a) to feed a cogeneration power plant for attending 3 MWe and 5.5 MWth capacity. Field data were collected on-site to calculate the boiler efficiency using the indirect method according to ASME PTC4 standard. The main components of the boiler were modeled using the OpenModelica® tool and the ThermoSysPro® library. The model accuracy was verified at different loads with the available steam generator measurement data and datasheets provided by the manufacturer. As a result, the model implemented allowed to reproduce the field data results for all studied partial loads. In the hybrid design, the boiler had a satisfactory thermodynamic behavior in the analyzed period, corresponding to a fuel saving of about 82.3 t/day (19.6%) for a clear day and 54.1 t/day (12.9%) for a cloudy day.*

Keywords: *Biomass steam generator, Cogeneration, Concentrated Solar Power, Hybrid systems, Part-load operation.*

1. INTRODUCTION

Biomass and solar energy have shown a significant increase in recent years in the Brazilian and also worldwide electrical matrix. Hybrid systems involving the use of biomass and solar energy have been proposed as a promising alternative to reduce emissions of greenhouse gases in the generation of heat and electricity.

Bioelectricity currently holds the fourth largest share in the supply of electricity in Brazil. In 2019, according to the National Energy Balance, biomass thermoelectric plants were responsible for the generation of 52.5 TWh, equivalent to about 8.4% of the total electricity supply in the country. In terms of installed capacity, considering centralized generation, biomass thermoelectric plants have the fourth largest share in the matrix, with 14970 MW, corresponding to 8.8% of the total installed capacity (EPE, 2020).

It is well known that Concentrated Solar Power (CSP) plants require abundant solar radiation to be profitable (Colmenar-Santos *et al.*, 2015), limiting implementation to remote areas and distant energy consumption centers. In addition, the intermittent nature of solar radiation accentuates the disadvantage of generation stability. To overcome such problems, CSP plants are generally designed with power capacities of the order of 100 MWel (Jin and Hong, 2012; Soares and Oliveira, 2017), with large capital investment and high financial risk.

Hybridization with biomass represents an ingenious way of meeting energy demand uninterruptedly. In addition to stability, hybridization allows for a fully renewable solution, while ensuring energy supply (Soares and Oliveira, 2017). The concept of CSP / biomass hybridization is based on the ability of the two systems to provide thermal energy to drive a power generation block continuously and without fluctuations. Other advantages of this synergy are operational stability and flexibility, shared use of plant equipment and associated cost savings, as well as enabling the migration of CSP plants

from desert areas to load centers (Cot *et al.*, 2010; Coelho *et al.*, 2012; Jin and Hong, 2012; Peterseim *et al.*, 2013, 2014; Colmenar-Santos *et al.*, 2015; Soares and Oliveira, 2017). Although the power dispatch capability has been widely proven in CSP systems with thermal energy storage (TES), it is still an expensive solution (Coelho, 2014; Soares and Oliveira, 2017; Suresh *et al.*, 2019).

During daylight periods, solar radiation is abundant and the system can operate at a higher solar fraction, resulting in a reduction in the Levelized Cost of Energy (LCOE). Nevertheless, when adding solar energy to the power cycle, some components of the plant should work in the off-design condition, penalizing their performance in partial loads. For example, the steam generator unit needs to adapt to fluctuations in the solar field and operate under variable load. Maintaining the boiler efficiency at an acceptable level is important from an energetic, economic, and even environmental point of view. Several studies on hybrid system design, optimization, and performance in the off-design condition have already been reported in the technical literature. However, the operation of biomass steam generating units in the hybrid design, in parallel with the solar field in the off-design condition, has not yet been discussed in sufficient depth (Datta *et al.*, 2010; Ahmadi *et al.*, 2012; Soltani *et al.*, 2013; Liu *et al.*, 2016; Pramanik and Ravikrishna, 2016; Yan *et al.*, 2020) and the measurements during the off-design operation from an existing real Combined Heat and Power (CHP) plant are seldom available in the literature.

This paper presents a proposal for hybrid solar-biomass integration using a field of Fresnel-type concentrators for generating superheated steam in parallel. The thermodynamic model of partial load analysis and the discussion of results of the simulations of the hybrid plant in the nominal and off-design conditions are described.

2. THE COGENERATION POWER PLANT

The cogeneration system here studied is an existing real plant and is based on a Rankine cycle. It consists of a biomass steam generator fueled with eucalyptus wood chips, a back-pressure steam turbine, a deaerator, pumps, and auxiliary components. The physical structure of the plant is shown in Fig. 1.

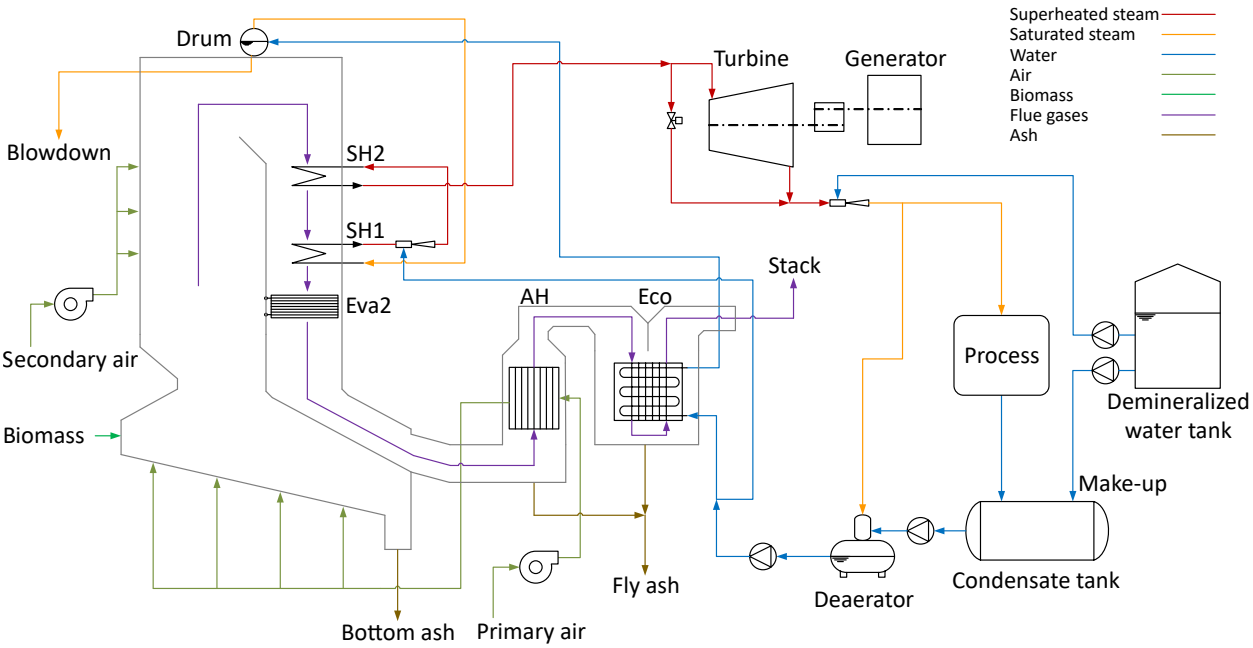

Figure 1: Schematic process diagram of the cogeneration plant.

The biomass steam generator provides superheated steam at 420 °C and 45 bar(a). It is designed with one drum connecting the water wall inside the furnace, two convective superheaters (SH1 and SH2), a secondary evaporator (EVA2), one air preheater (AH), and one economizer (ECO). The furnace is partially covered with refractory bricks, forming a radiant surface suitable for biomass combustion over a reciprocating grate. The superheaters consist of a bundle of aligned tubes and are located after the furnace in the convective pass. The temperature control of the superheated steam is performed through the direct injection of liquid water in between SH1 and SH2. This control keeps the steam temperature within acceptable limits, to correct the fluctuations caused by instabilities during boiler operation. The air preheater consists of vertical scattered tubes, through which the flue gas passes internally. The economizer consists of a bundle of finned tubes. The superheated steam is conducted to the back-pressure steam turbine where it is expanded up to 10 bar(a) to supply the process steam demand (5.5 MWth). The turbine is coupled to a synchronous electricity generator with a nominal power capacity of 3 MWe that supplies part of the electrical energy demand of the industry in which the

cogeneration plant is installed.

3. THE SOLAR-AIDED PLANT CONCEPT

The conceptual scheme of the proposed solar-biomass hybrid system is presented in Fig. 2. In the proposed concept, the biomass steam generator is operated in parallel with a linear Fresnel solar field. Under the hybrid operation, while steam is generated in the solar field during sunny hours, the thermal load of the biomass steam generator is modulated to keep the superheated steam mass flow as required by the process. The Fresnel solar field provides direct steam generation (DSG), and it is equipped with Nova-1 and Supernova concentrators in the evaporation and superheating sections, respectively (Novatec Solar, 2014). Components that also integrate the solar field are recirculation pumps, liquid/vapor separators, and liquid injectors for superheated steam temperature control (attemperators). Figure 3 shows the schematic process diagram for one collector row. The solar field is sized to provide up to 60% of the total power block superheated steam demand at design point operation.

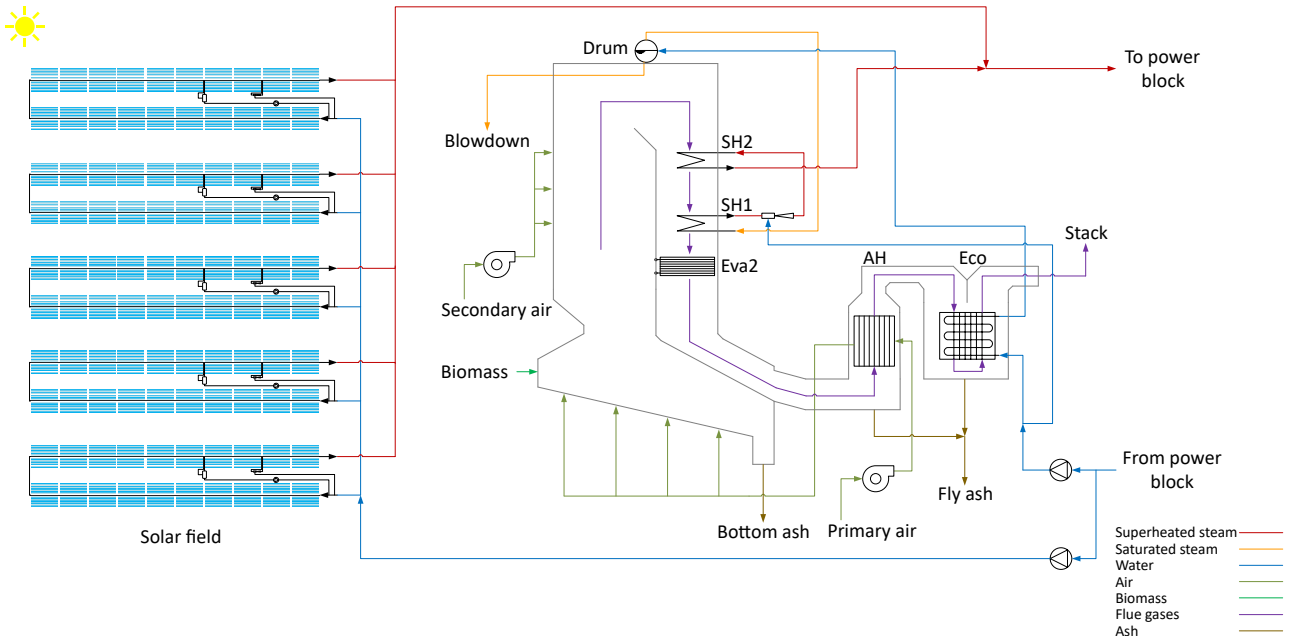

Figure 2: Schematic process diagram of the proposed solar-biomass hybrid plant.

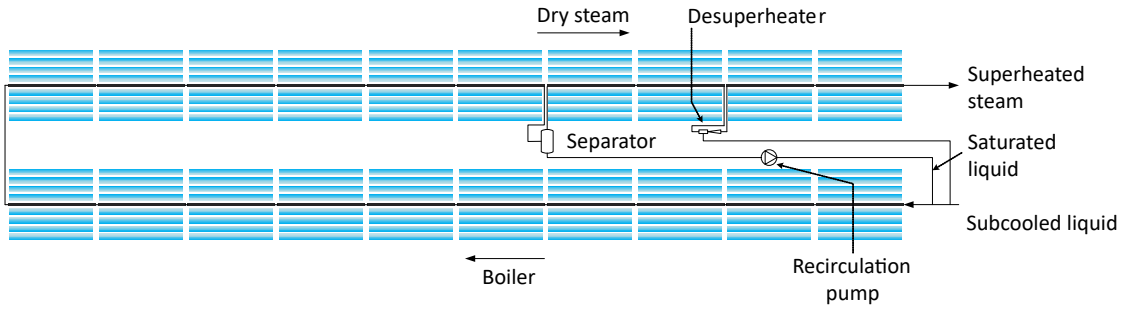

Figure 3: Schematic process diagram for one collector row.

4. DATA COLLECTION AND STEAM BOILER EFFICIENCY CALCULATION

Field data were collected on-site considering the operation at different partial loads. To reproduce the thermodynamic behavior of the steam generating unit, the energy efficiency calculation method was carried out according to procedures established by the ASME PTC 4 (2013) standard, adopting as simplifying assumptions:

a. steady-state operation;

b. the fuel elemental composition (as shown in Tab. 1) and Lower Heating Value (LHV) of 9850 kJ/kg, according to manufacturer's specifications;

c. the bottom and fly ash flow rates were calculated based on the ash content and amount of burned fuel;

d. the fly ash share was considered equal to 30%;
e. heat loss through the walls in the order of 1% of the available energy in the furnace, at nominal load;
f. purge losses estimated according to the boiler mass balance;
g. soot blowers and auxiliary services losses on the order of 1% of the available energy;
h. the presence of unburned carbon is about 20% in the ashtray.

The equations established by the ASME PTC 4 (2013) standard were all implemented in Phyton (PSF, 2020).

Table 1: Mass fractions of the eucalyptus woodchips.

Symbol	**C**	**H**	**O**	**N**	**S**	**W**	**Ash**
%mass	30.0	4.0	25.2	0.1	0.0	40.0	0.7

Table 2 shows the data collected on-site during the test runs used to calculate the efficiency of the steam generating unit, for loads ranging from 40 to 85%. The flue gas composition was determined using an MRU Optima7® flue gas analyzer and the samples were taken before the air preheater to avoid oxygen infiltration. The corresponding data of temperature, pressure, and mass flow rates were collected from the supervisory system. It is important to highlight that in the runs performed to calculate the thermal efficiency of the steam generator, the steam mass flow rate varied according to the industrial process demand. The procedure adopted consisted of monitoring the operation of the plant over three days and selecting periods in which the operating parameters of the unit were the closest to what characterizes the operation of a steam generator on steady-state conditions, according to ASME PTC 4 (2013) standard.

Table 2: Data collected for steam generator efficiency calculation.

	Load 40%	**Load 55%**	**Load 75%**	**Load 80%**	**Load 85%**
Primary air temperature, °C	104.6	90.4	124.6	136.2	135.8
Secondary air temperature, °C	25.0	25.0	25.0	25.0	25.0
Temperature of flue gas leaving stack, °C	199.9	168.0	175.1	180.6	180.6
Temperature of superheated steam, °C	394.0	400.4	412.0	415.5	416.7
Feedwater temperature, °C	105.4	104.1	93.9	94.0	94.1
Desuperheater water temperature, °C	105.4	104.1	93.9	94.0	94.1
O_2 in flue gas, %vol (dry basis)	7.13	4.83	7.09	5.94	3.89
CO_2 in flue gas, %vol (dry basis)	12.42	14.79	12.35	13.39	15.46
CO in flue gas, %vol (dry basis)	0.33	0.66	0.10	0.08	0.33
Excess air, %	50.8	29.5	50.3	39.0	22.4
Mass fraction of moisture in dry air, kg/kg	0.016	0.016	0.016	0.016	0.016
Mass flow rate of dry air, kg/s	11.3	12.8	20.3	20.1	18.7
Mass flow rate of wet air, kg/s	11.4	13.0	20.6	20.5	19.0
Mass flow rate of wet flue gas, kg/s	13.4	15.6	24.2	24.3	23.1
Mass flow rate of bottom ash, kg/s	0.012	0.016	0.022	0.024	0.025
Mass flow rate of fly ash, kg/s	0.005	0.007	0.010	0.010	0.011
Unburned carbon in fuel, %mass	0.175	0.175	0.175	0.175	0.175

The Sankey diagrams (Fig. 4 and 5) show the results concerning the steam generator's thermal efficiency based on the fuel LHV. The strong efficiency reduction at partial loads was mainly caused by the increase in thermal losses associated with flue gas stack, wet flue gas, heat transfer to the environment (relative to the available energy at the furnace), and carbon monoxide emission.

The efficiency results for the steam generator unit are presented in Fig. 6. As can be seen, the results are in good agreement with the maximum and minimum efficiency expected values provided by the manufacturer. It is important to note that a reduction in produced steam mass flow does not imply a reduction in fuel consumption in the same proportion. In this work, the minimum load of the steam generating unit is limited to 40%, a situation in which the solar field will operate at its nominal load, producing 60% of the steam demanded by the power block.

5. THERMODYNAMIC MODEL FOR ANALYSIS OF THE PROPOSED POWER PLANT

5.1 Cogeneration plant model

The implemented model is based on the non-commercial Modelica ThermoSysPro Library v3.2 (EDF, 2019) components. The simulations were performed in OpenModelica OMEdit Editor v1.17 (OSMC, 2021) (Fig. 7) and using as inputs design data provided by the manufacturer and collected field operation data.

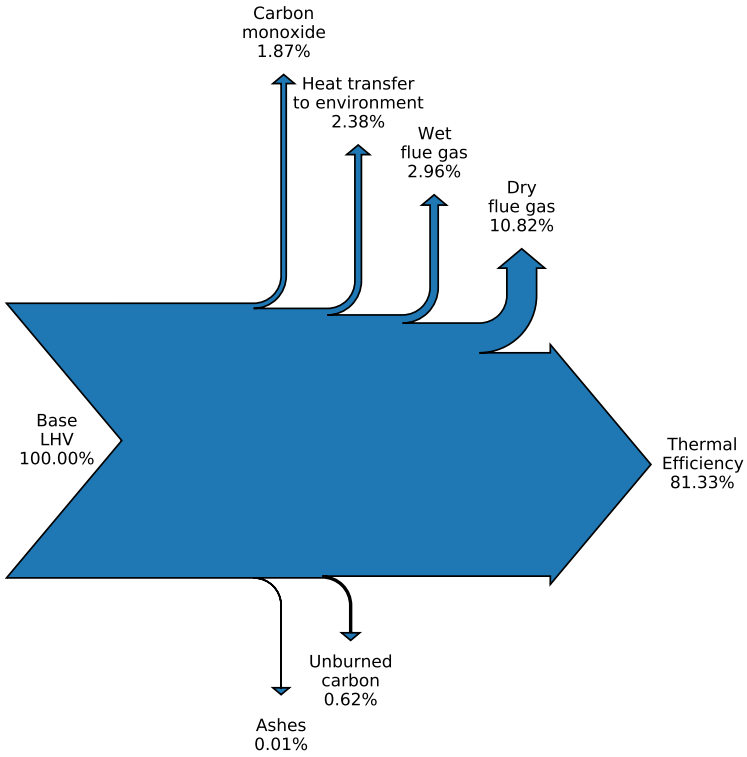

Figure 4: Sankey diagram for heat losses at 40% load.

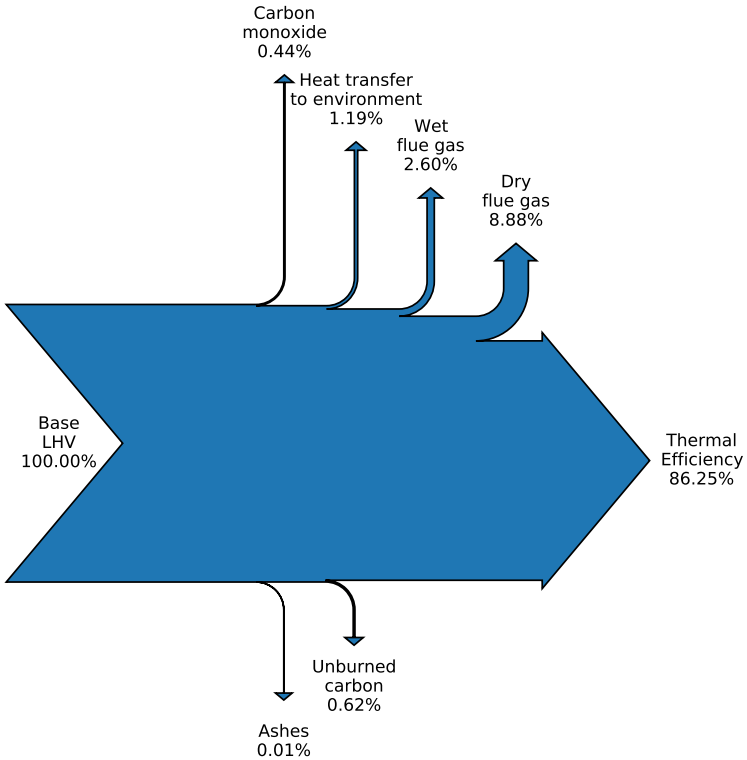

Figure 5: Sankey diagram for heat losses at 80% load.

The combustion chamber was modeled using the *GenericCombustion1D* component. Thus, no accumulation of mass and energy in the control volume was considered and the radiative and convective heat exchange between the flue gas and the water wall was modeled in one dimension along the gas flow path. Water walls were modeled using the *DynamicTwoPhaseFlowPipe* and *HeatExchangerWall* components. The boiler drum was modeled using the *DynamicDrum* component, which consists of the non-equilibrium two-phase formulation of the fluid balance equations, and considers the heat transfer between (1) the liquid and vapor phases, (2) the fluid and the drum wall, and (3) the drum and the external

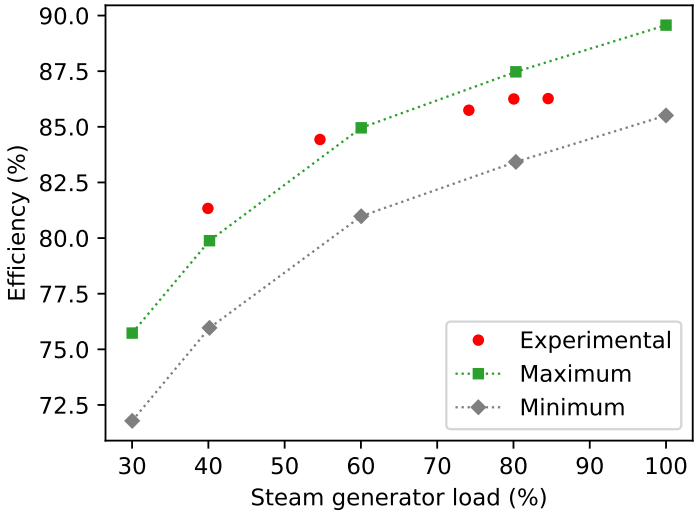

Figure 6: Biomass steam generator efficiency at part-loads.

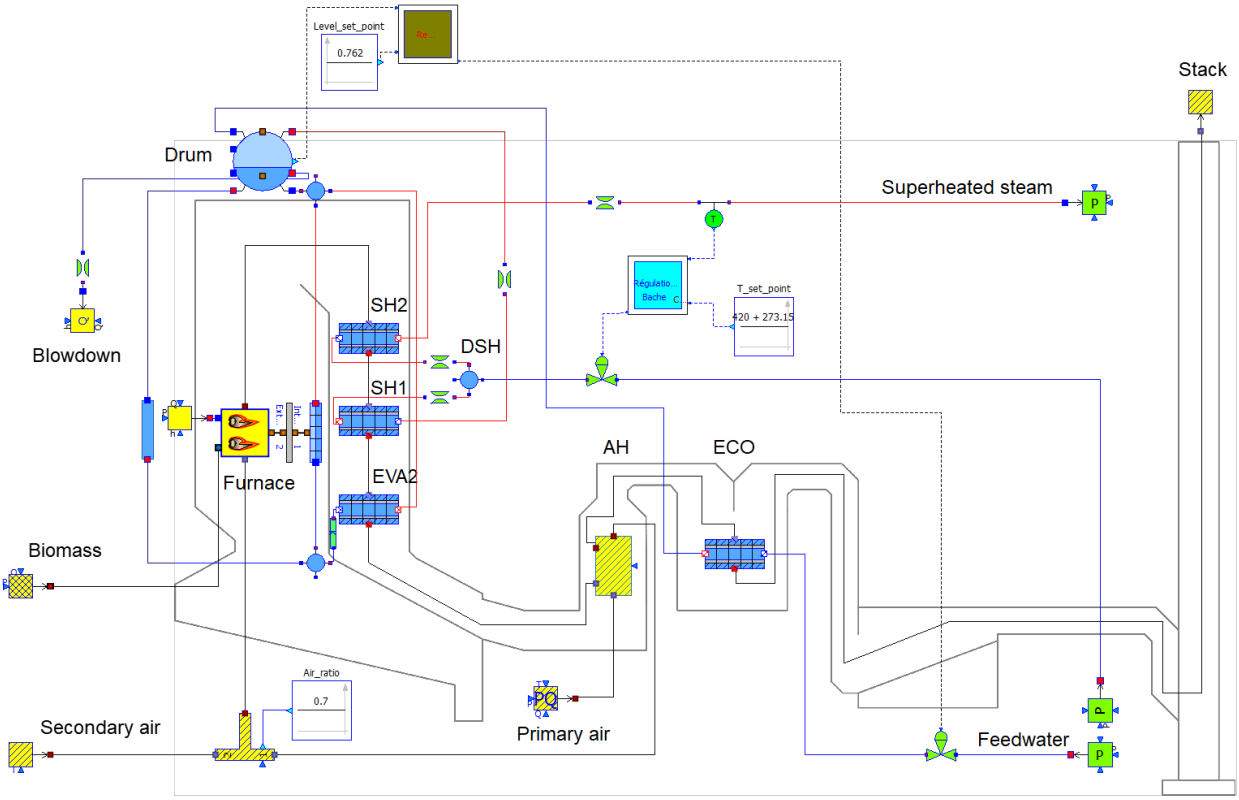

Figure 7: Schematic Modelica process model diagram of the biomass steam generator.

medium. The superheaters, the secondary evaporator, and economizer heat exchangers were all modeled by using the *DynamicExchangerWaterSteamFlueGases* heat exchanger model. Under these models, 1-D discretization is performed in the flow direction and both internal and external effective design point pressure drops are defined as inputs. The thermal inertia of metals was estimated using the metal tube model *HeatExchangerWall* discretized in the flow direction. The air heater was modeled using the *StaticFluegasesFluegasesExchangerKS* component as a basis. This component has been modified to be able to calculate the global heat transfer coefficient at part-load. The correlation proposed by Manente *et al.* (2013) was considered in this study, to account for the off-design behavior of the heat exchanger. All component models are described in El Hefni and Bouskela (2019).

5.2 Linear Fresnel solar field model

The general assumptions adopted for the solar field sizing are presented in Tab. 3. The simulation was performed for the city of Itaúna – MG, where the cogeneration power plant is installed. Design point of Direct Normal Irradiance (DNI) was defined calculating the 95% upper percentile, neglecting irradiance values smaller than 250 W/m². A similar approach was implemented for the design point ambient dry-bulb (DB) temperature. Temperature values in which DNI < 250 W/m² were not considered in calculations. The design point day was considered as the spring equinox in the southern hemisphere (22th September) (BURIN, 2015; Wang, 2019). Meteorological data were taken from the Solar and Wind Energy Resource Assessment (SWERA) project considering one-hour time steps (SWERA-NREL, 2011).

Table 3: Solar field sizing assumptions for simulation.

Parameter	**Adopted assumption**
Latitude, °	19.9227 S
Longitude, °	43.9450 W
Reference longitude, °	45 W
Design point irradiance, W/m²	880
Design point ambient temperature, °C	31 (DB)
TMY data	SWERA (Belo Horizonte – Brazil)
Time resolution	1-hour

Solar field design parameters are presented in Tab. 4. The configuration of each loop was determined for the solar field to generate superheated steam at 420 °C and 45 bar(a), while the number of loops was defined based on the required capacity of the solar field (30 t/h). The peak optical efficiency of the Linear Fresnel Reflector (LFR) and incidence angle modifiers (IAM) are available from the manufacturer. Similarly, the optical efficiency, heat loss, and total thermal output were calculated according to Novatec Solar datasheets (Novatec Solar, 2014).

Table 4: Main design parameters of the solar field.

Parameter	
Number of evaporator modules per row	16
Number of superheater modules per row	4
Total number of modules per row	20
Number of rows (loops)	5
Single loop aperture area, m²	10272
Steam pressure, bar	45
Steam temperature, °C	420
Steam mass flow rate per loop, t/h	6.2
Field steam mass flow rate, t/h	30.8
Feedwater inlet pressure, bar	55
Solar field pressure drop, bar	10
Feedwater inlet temperature, °C	130

The implemented model for the solar field simulation was also based on the Modelica ThermoSysPro Library components v3.2 (EDF, 2019) and using design data provided by the manufacturer. The evaporation and superheating sections of each solar field loop were both modeled using the *FresnelField* component, while absorbers were modeled using the *HeatExchangerWall* and *DynamicTwoPhaseFlowPipe* blocks. A schematic representation of the Fresnel model is presented in Fig. 8. All components are described in El Hefni and Bouskela (2019).

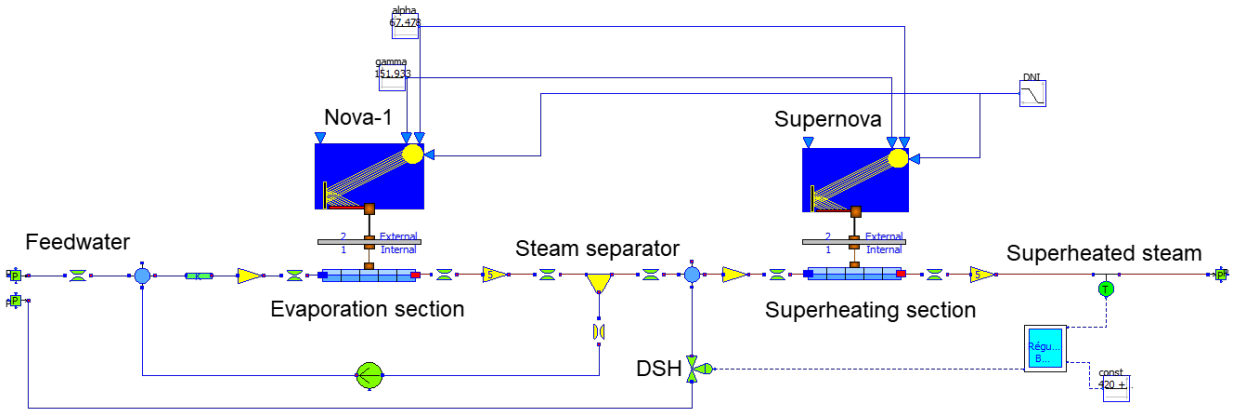

Figure 8: Schematic of the Modelica process model diagram for one collector row.

6. RESULTS AND DISCUSSION

6.1 Steam generator model checking

In Tab. 5, the results generated by the model implemented for simulation of the steam generating unit are compared with data collected for loads of 40 and 80%. The design data for 100% load were provided by the manufacturer. In general, it is observed a good adherence of the model to the measured data. The found difference of the exhaust gas temperature after the economizer was justified by the dynamic operation of the steam generating unit in responding to changes in steam consumption in the industrial unit, as shown in Tab. 2, where the volume fraction of oxygen in the exhaust gases varies in the range of 4.8 to 7.3%. This demonstrates a typical behavior in the combustion air control system of wood chip burning processes on a grate. The differences found in the gas temperature are reflected throughout the entire gas path. All remaining values showed good correspondence.

Table 5: Main simulation results.

Load	**40%**		**80%**		**100% (design)**	
Variable	Ref.	Model	Ref	Model	Ref.	Model
Steam temp. at SH2 outlet, °C	394.0	386.1	415.5	420.1	420.0	420.0
Steam temp. at attemperator outlet, °C	276.4	317.6	301.2	335.4	327.0	331.3
Steam temp. at SH1 outlet, °C	320.5	317.6	330.4	342.0	373.0	351.6
Steam temp. at drum outlet, °C	251.1	258.5	254.6	261.3	267.0	262.7
Water temp. at ECO outlet, °C	117.2	147.1	120.5	152.1	202.0	158.7
Flue gases temp. at SH2 outlet, °C	-	499.5	-	606.2	680.0	632.7
Flue gases temp. at SH1 outlet, °C	377.0	408.3	462.5	492.1	561.0	523.8
Flue gases temp. at EVA2 outlet, °C	304.1	286.4	362.3	323.7	352.0	345.3
Flue gases temp. at AH outlet, °C	277.7	232.4	319.2	258.5	283.0	272.0
Flue gases temp. at ECO outlet, °C	199.9	158.6	180.6	173.0	157.0	185.7

6.2 Solar field model checking

Results were verified by comparison to System Advisor Model (SAM) results, free software developed by the National Renewable Energy Laboratory (NREL) (NREL, 2020). The superheated steam mass flow produced by the solar field is shown in Fig. 9 and 10, according to the direct solar irradiance on a clear day (2nd Sep) and a cloudy day (21st Oct), respectively.

Although the solar field was sized to generate up to 60% of the steam demanded by the cogeneration unit (30 t/h), on the clear day when the direct radiation exceeded 880 W/m² (design point), the solar field steam output overcame 32 t/h. Thus, when the hybrid plant is operated, the need to partially defocus mirrors should always be evaluated to adjust the steam generation to a safe condition. During the cloudy day, the solar field was able to generate superheated steam according to the DNI variations. It is also observed that there is a delay between the start of steam generation and the incidence of radiation at the beginning of the day. This period is dependent on the inertia of components and the available solar radiation. During power plant start-up, there is a period when solar radiation is not enough to begin generating steam (Coelho *et al.*, 2014; Wagner and Zhu, 2012).

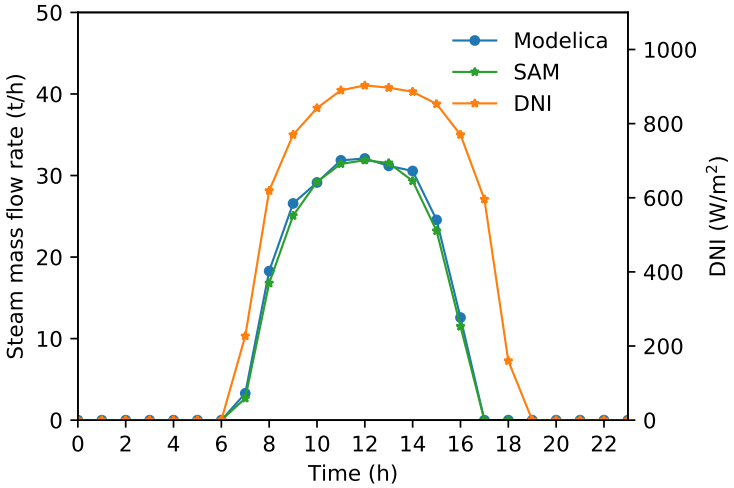

Figure 9: Solar field simulation results for a clear day (2nd Sep).

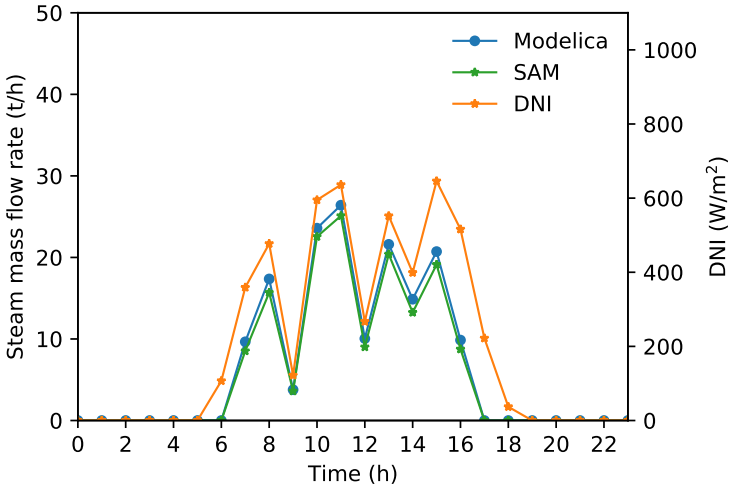

Figure 10: Solar field simulation results for a cloudy day (21st Oct).

6.3 Solar-aided plant simulation

In Fig. 11 and 12 are presented the simulation results of the hybrid solar-biomass plant under varying solar radiation during a clear day (2nd Sep) and a cloudy day (21st Oct). The biomass steam generator is operated for 24h with variation in load during daytime hours (partial load) and constant load during nighttime (full load). The maximum steam mass flow rates generated in the solar field are 32.1 and 26.4 t/h during a clear and cloudy day, respectively. The minimum value of steam mass flow rates in the biomass steam generator are 17.9 and 23.6 t/h during a clear and cloudy day, respectively. The minimum allowable steam generation recommended by the manufacturer is 13 t/h. For these specific days, the load on the steam generator did not exceed the lower limit. However, it is again evident that a control system that limits the maximum steam generation in the solar field is needed to prevent the operation of the steam generator at loads lower than the minimum recommended by the manufacturer.

It is presented in Fig. 13 and 14 the eucalyptus wood chips consumption during hybrid operation in fuel-saving mode. The minimum fuel supplies to the combustion chamber are 6.5 and 8.4 t/h during a clear and cloudy day, respectively. The fuel saved was 19.6 during a clear day and 12.9% during a cloudy day.

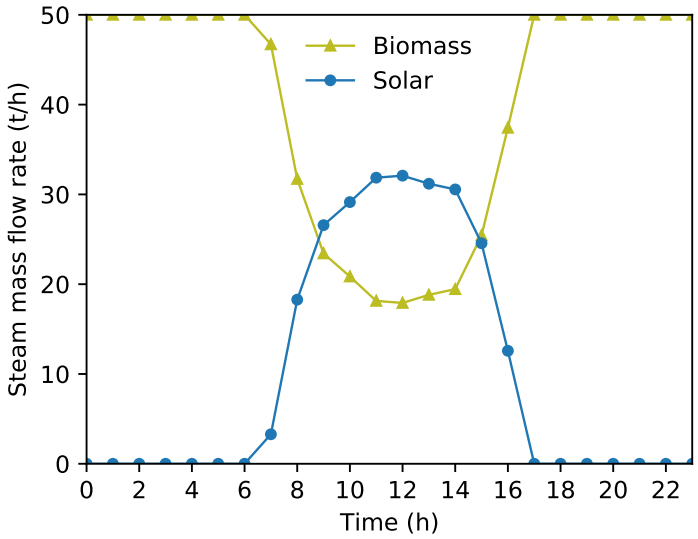

Figure 11: Solar-aided plant simulation results for a clear day (2nd Sep).

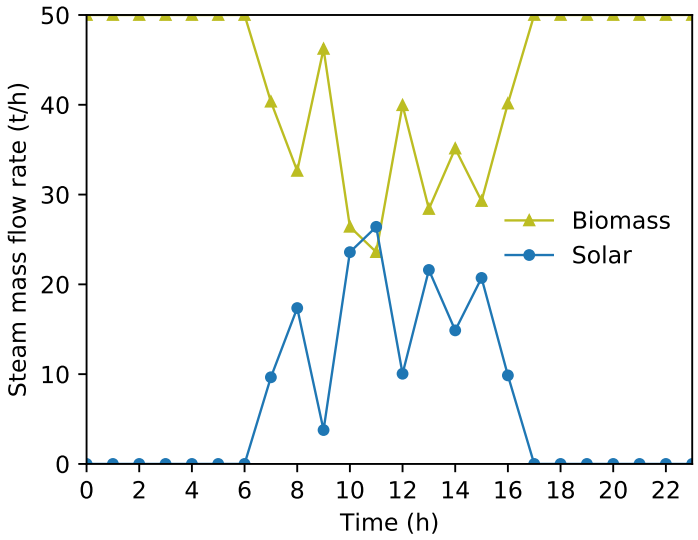

Figure 12: Solar-aided plant simulation results for a cloudy day (21st Oct).

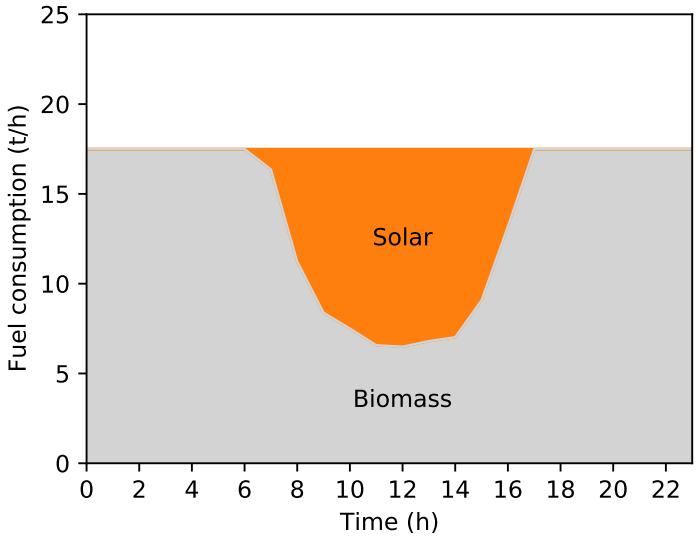

Figure 13: Biomass consumption for a clear day (2nd Sep).

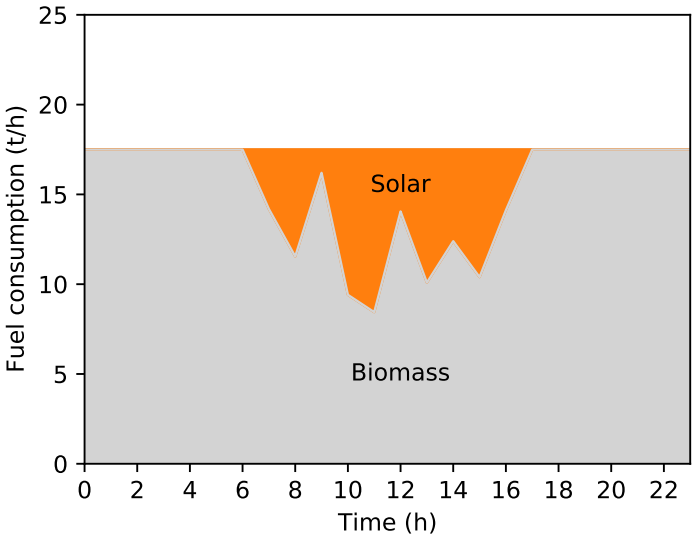

Figure 14: Biomass consumption for a cloudy day (21st Oct).

7. CONCLUSION

The model implemented to simulate the operation of the biomass steam generator unit allowed to reproduce the field data results at different steady-state base loads.

Similarly, a simulation model was implemented for a linear Fresnel solar field, which allowed to reproduce the steam generation curve over a clear day and a cloudy day. Simulation results show that the applied solar field is able to produce superheated steam at desired stable conditions under different irradiation levels.

In the hybrid design, the boiler had a satisfactory thermodynamic behavior in the analyzed periods, corresponding to a fuel saving of about 82.3 t/day (19.6%) for a clear day and 54.1 t/day (12.9%) for a cloudy day.

Further studies are still needed to effectively assess the technical feasibility of hybrid electricity generation combining biomass and solar thermal energy as primary energy sources. The results obtained so far are promising, and the next steps are to analyze the operation of the hybrid plant for typical meteorological years in different locations in Brazil and the world. Measurements during the off-design operation from an existing real CHP plant are presented in this paper, which is of high importance since such data is seldom available in the literature.

8. ACKNOWLEDGEMENTS

The authors acknowledge ICAVI company for providing technical data, the Coordination for the Improvement of Higher Education Personnel (CAPES), National Council for Scientific and Technological Development (CNPq), and Araucaria Foundation (CP 20/2018 PPP - contract number 047/2020) for the financial support.

9. REFERENCES

Ahmadi, P., Rosen, M.A. and Dincer, I., 2012. "Multi-objective exergy-based optimization of a polygeneration energy system using an evolutionary algorithm". *Energy*, Vol. 46, No. 1, pp. 21–31. ISSN 03605442. doi:10.1016/j.energy.2012.02.005. URL `http://dx.doi.org/10.1016/j.energy.2012.02.005` `https://linkinghub.elsevier.com/retrieve/pii/S0360544212000990`.

ASME PTC 4, 2013. *Fired Steam Generators, Performance Test Code (Revision of ASME PTC 4-2008)*. The American Society of Mechanical Engineers, New York. ISBN 9780791868997.

BURIN, E.L.K., 2015. *Plantas de cogeração do setor sucroalcooleiro assistidas por concentradores parabólicos*. Ph.D. thesis, Doctoral Thesis, Federal University of Santa Catarina (UFSC), Florianópolis.

Coelho, B., 2014. *Study of a hybrid concentrating solar power plant for Portuguese conditions*. Ph.D. thesis.

Coelho, B., Schwarzbözl, P., Oliveira, A. and Mendes, A., 2012. "Biomass and central receiver system (CRS) hybridization: Volumetric air CRS and integration of a biomass waste direct burning boiler on steam cycle". *Solar Energy*, Vol. 86, No. 10, pp. 2912–2922. ISSN 0038092X. doi:10.1016/j.solener.2012.06.009.

Coelho, B., Varga, S., Oliveira, A. and Mendes, A., 2014. "Optimization of an atmospheric air volumetric central receiver system: Impact of solar multiple, storage capacity and control strategy". *Renewable Energy*, Vol. 63, pp. 392–401. ISSN 09601481. doi:10.1016/j.renene.2013.09.026. URL `http://dx.doi.org/10.1016/j.renene.2013.09.026`.

Colmenar-Santos, A., Bonilla-Gómez, J., Borge-Diez, D. and Castro-Gil, M., 2015. "Hybridization of concentrated solar power plants with biogas production systems as an alternative to premiums: The case of Spain". *Renewable and Sustainable Energy Reviews*, Vol. 47, pp. 186–197. ISSN 18790690. doi:10.1016/j.rser.2015.03.061. URL http://dx.doi.org/10.1016/j.rser.2015.03.061.

Cot, A., Ametller, A., Vall-Llovera, J., Aguiló, J. and Arqué, J.M., 2010. "Termosolar Borges: A thermosolar hybrid plant with biomass".

Datta, A., Ganguly, R. and Sarkar, L., 2010. "Energy and exergy analyses of an externally fired gas turbine (EFGT) cycle integrated with biomass gasifier for distributed power generation". *Energy*, Vol. 35, No. 1, pp. 341–350. ISSN 03605442. doi:10.1016/j.energy.2009.09.031. URL http://dx.doi.org/10.1016/j.energy.2009.09.031 https://linkinghub.elsevier.com/retrieve/pii/S0360544209004241.

EDF, 2019. "ThermoSysPro, version 3.2, 2019".

El Hefni, B. and Bouskela, D., 2019. *Modeling and Simulation of Thermal Power Plants with ThermoSysPro*. Springer International Publishing, Cham.

EPE, 2020. *Brazilian Energy Balance 2020 Year 2019*. EPE, Rio de Janeiro.

Jin, H. and Hong, H., 2012. "Hybridization of concentrating solar power (CSP) with fossil fuel power plants". In K. Lovegrove and W. Stein, eds., *Concentrating Solar Power Technology*, Woodhead Publishing, 2012, pp. 395–420. doi:10.1533/9780857096173.2.395. URL https://linkinghub.elsevier.com/retrieve/pii/B9781845697693500121.

Liu, M., Steven Tay, N.H., Bell, S., Belusko, M., Jacob, R., Will, G., Saman, W. and Bruno, F., 2016. "Review on concentrating solar power plants and new developments in high temperature thermal energy storage technologies". *Renewable and Sustainable Energy Reviews*, Vol. 53, pp. 1411–1432. ISSN 18790690. doi:10.1016/j.rser.2015.09.026. URL http://dx.doi.org/10.1016/j.rser.2015.09.026.

Manente, G., Toffolo, A., Lazzaretto, A. and Paci, M., 2013. "An Organic Rankine Cycle off-design model for the search of the optimal control strategy". *Energy*, Vol. 58, pp. 97–106. ISSN 03605442. doi:10.1016/j.energy.2012.12.035. URL http://dx.doi.org/10.1016/j.energy.2012.12.035.

Novatec Solar, 2014. "Turnkey Solar Boiler, based on Fresnel Collector Technology, mass produced in industrial precision with performance guarantee". Technical report.

NREL, 2020. "System Advisor Model (SAM), version 2020.11.29 Revision 2".

OSMC, 2021. "OpenModelica, version 1.16.5, 2021".

Peterseim, J.H., Herr, A., Miller, S., White, S. and O'Connell, D.A., 2014. "Concentrating solar power/alternative fuel hybrid plants: Annual electricity potential and ideal areas in Australia". *Energy*, Vol. 68, pp. 698–711. ISSN 03605442. doi:10.1016/j.energy.2014.02.068. URL http://dx.doi.org/10.1016/j.energy.2014.02.068.

Peterseim, J.H., White, S., Tadros, A. and Hellwig, U., 2013. "Concentrated solar power hybrid plants, which technologies are best suited for hybridisation?" *Renewable Energy*, Vol. 57, pp. 520–532. ISSN 09601481. doi:10.1016/j.renene.2013.02.014. URL http://dx.doi.org/10.1016/j.renene.2013.02.014.

Pramanik, S. and Ravikrishna, R., 2016. "A novel syngas-fired hybrid heating source for solar-thermal applications: Energy and exergy analysis". *Applied Thermal Engineering*, Vol. 109, pp. 1011–1022. ISSN 13594311. doi:10.1016/j.applthermaleng.2016.04.139. URL http://dx.doi.org/10.1016/j.applthermaleng.2016.04.139 https://linkinghub.elsevier.com/retrieve/pii/S1359431116306275.

PSF, 2020. "Python Language Reference, version 3.8.5, 2020".

Soares, J. and Oliveira, A.C., 2017. "Numerical simulation of a hybrid concentrated solar power/biomass mini power plant". *Applied Thermal Engineering*, Vol. 111, pp. 1378–1386. ISSN 13594311. doi:10.1016/j.applthermaleng.2016.06.180.

Soltani, S., Mahmoudi, S., Yari, M., Morosuk, T., Rosen, M. and Zare, V., 2013. "A comparative exergoeconomic analysis of two biomass and co-firing combined power plants". *Energy Conversion and Management*, Vol. 76, pp. 83–91. ISSN 01968904. doi:10.1016/j.enconman.2013.07.030. URL http://dx.doi.org/10.1016/j.enconman.2013.07.030 https://linkinghub.elsevier.com/retrieve/pii/S0196890413004019.

Suresh, N., Thirumalai, N. and Dasappa, S., 2019. "Modeling and analysis of solar thermal and biomass hybrid power plants". *Applied Thermal Engineering*, Vol. 160, No. June, p. 114121. ISSN 13594311. doi:10.1016/j.applthermaleng.2019.114121. URL https://doi.org/10.1016/j.applthermaleng.2019.114121 https://linkinghub.elsevier.com/retrieve/pii/S1359431118335956.

SWERA-NREL, 2011. "Solar and wind energy resource assessment - SWERA". URL https://openei.org/doe-opendata/dataset/swera.

Wagner, M.J. and Zhu, G., 2012. "A Direct-Steam Linear Fresnel Performance Model for NREL's System Advisor Model". *ASME 2012 6th International Conference on Energy Sustainability Parts A B*, pp. 459–468. doi:10.1115/ES2012-91317.

Wang, Z., 2019. *Design of Solar Thermal Power Plants*. Elsevier, Inc., London, 1st edition.

Yan, H., Li, X., Liu, M., Chong, D. and Yan, J., 2020. "Performance analysis of a solar-aided coal-fired power plant in off-design working conditions and dynamic process". *Energy Conversion and Management*, Vol. 220, No. June, p. 113059. ISSN 01968904. doi:10.1016/j.enconman.2020.113059. URL https://doi.org/10.1016/j.enconman.2020.113059.